Article:
Bussotti, Giovanni, Gouzelou, Evi, Cortes Boite, Mariana et al. (27 more authors) (2018) Leishmania genome dynamics during environmental adaptation reveals strain-specific differences in gene copy number variation, karyotype instability, and telomeric amplification. MBio. e01399-18. ISSN: 2150-7511

https://doi.org/10.1128/mBio.01399-18

Leishmania genome dynamics during environmental adaptation reveals strain-specific differences in gene copy number variation, karyotype instability, and telomeric amplification

Giovanni Bussotti[1,2], Evi Gouzelou[2], Mariana Côrtes Boité[3],Ihcen Kherachi[4], Zoubir Harrat[4], Naouel Eddaikra[4], Jeremy C. Mottram[5], Maria Antoniou[6], Vasiliki Christodoulou[6], Aymen Bali[7,8], Fatma Z Guerfali[7,8], Dhafer Laouini[7,8], Maowia Mukhtar[9], Franck Dumetz[10], Jean-Claude Dujardin[10,11], Despina Smirlis[12], Pierre Lechat[1], Pascale Pescher[2], Adil El Hamouchi[13], Meryem Lemrani[13], Carmen Chicharro[14], Ivonne Pamela Llanes-Acevedo[14], Laura Botana[14], Israel Cruz[14], Javier Moreno[14],Fakhri Jeddi[8,15], Karim Aoun[8,15], Aïda Bouratbine[8,15], Elisa Cupolillo[3] and Gerald F. Späth[2,*]

[1]Institut Pasteur – Bioinformatics and Biostatistics Hub – C3BI, USR 3756 IP CNRS – Paris, France; [2]Unité de Parasitologiemoléculaire et Signalisation, Institut Pasteur, Paris, France; [3]Laboratory on Leishmaniasis Research, Oswaldo Cruz Institute-Fiocruz, Rio de Janeiro, Brazil; [4]Laboratoire d'Eco-épidémiologieparasitaire et Génétique des populations, Institut Pasteur d'Alger, Alger, Algérie; [5]Centre for Immunology and Infection, Department of Biology, University of York, United Kingdom; [6]Laboratory of Clinical Bacteriology, Parasitology, Zoonoses and Geographical Medicine, School of Medicine, University of Crete, VassilikaVouton, Heraklion, Greece; [7]Institut Pasteur de Tunis, LR11IPT02, Laboratory of Transmission, Control and Immunobiology of Infections (LTCII), Tunis-Belvédère, Tunisia; [8]Université Tunis El Manar, Tunis, Tunisia; [9]The Institute of Endemic Diseases, University of Khartoum, Sudan; [10]Molecular Parasitology Unit, Institute of Tropical Medicine, Antwerp, Belgium; [11]Department of Biomedical Sciences, University of Antwerp, Belgium; [12]Molecular Parasitology Laboratory, Microbiology Department, Hellenic Pasteur Institute, Athens,

Greece; [13]Laboratory of Parasitology and Vector-Borne-Diseases, Institut Pasteur du Maroc, Casablanca, Morocco; [14]WHO Collaborating Centre for Leishmaniasis,Instituto de Salud Carlos III, Madrid, Spain; [15]Institut Pasteur de Tunis, LR11IPT06, Reasearch Laboratory "Medical Parasitology, Biotechnology and Biomolecules",Tunis-Belvédère, Tunisia

* To whom correspondence should be addressed. Tel: +33.1.40.61.38.58; Fax: +33.1.45.68.83.32; Email: gerald.spaeth@pasteur.fr

Abstract

Protozoan parasites of the genus *Leishmania* adapt to environmental change through chromosome and gene copy number variations. Only little is known on external or intrinsic factors that govern *Leishmania* genomic adaptation. Here, by conducting longitudinal genome analyses of ten new *Leishmania* clinical isolates, we uncovered important differences in gene copy number among genetically highly related strains and revealed gain and loss of gene copies as potential drivers of long-term environmental adaptation in the field. In contrast, chromosome rather than gene amplification was associated with short-term environmental adaptation to *in vitro* culture. Karyotypic solutions were highly reproducible but unique for a given strain, suggesting that chromosome amplification is under positive selection and dependent on species- and strain-specific, intrinsic factors. We revealed a progressive increase in read depth towards the chromosome ends for various *Leishmania* isolates, which may represent a non-classical mechanism of telomere maintenance that can preserve integrity of chromosome ends during selection for fast *in vitro* growth. Together our data draw a complex picture of *Leishmania* genomic adaptation in the field and in culture, which is driven by a combination of intrinsic genetic factors that generate strain-specific, phenotypic variations, which are under environmental selection and allow for fitness gain.

Importance

Protozoan parasites of the genus *Leishmania* cause severe human and veterinary diseases world-wide, termed leishmaniases. A hallmark of *Leishmania* biology is its capacity to adapt to a variety of unpredictable fluctuations inside its human host, notably pharmacological interventions thus causing drug resistance. Here we investigated mechanisms of environmental adaptation using a comparative genomics approach by sequencing ten new clinical isolates of the *L. donovani, L. major,* and *L. tropica* complexes that were sampled across eight distinct geographical regions. Our data provide new evidence that parasites

adapt to environmental change in the field and in culture through a combination of chromosome and gene amplification that likely causes phenotypic variation and drives parasite fitness gains in response to environmental constraints. This novel form of gene expression regulation through genomic change compensates for the absence of classical transcriptional control in these early-branching eukaryotes and opens new venues for biomarker discovery.

Introduction

Protozoan parasites of the genus *Leishmania* are transmitted by female blood-feeding sand flies and can cause severe diseases in infected humans and animals. The success of this pathogen relies on its capacity to sense changes in various host environments that trigger various developmental transitions (1). Inside phlebotomine insect vectors, non-infectious procyclic promastigote parasites differentiate into highly infectious metacyclic promastigotes, which are transmitted to vertebrate hosts during a blood meal, where they develop into the disease-causing amastigote form inside host macrophages (2, 3). Aside from stage differentiation, *Leishmania* seem to adapt to a variety of environmental fluctuations encountered in their hosts with important consequences for infection outcome, such as drug treatment. Phenotypic shifts in *Leishmania* have been linked to genome plasticity, with frequent copy number variations (CNVs) of individual genes or chromosomes linked to drug resistance (4-9) or tissue tropism (10, 11). A better insight into molecular and genetic mechanisms underlying *Leishmania* genetic diversity and evolution of new phenotypes is therefore essential to understand parasite pathogenicity and hence the epidemiology of *Leishmania* infection.

Combining DNAseq and RNAseq analyses of karyotypically distinct *L. donovani* field isolates and experimental clones, we recently established a direct correlation between transcript abundance and chromosome amplification (12, 13) - a form of genomic regulation of gene expression levels that compensates for the absence of classical transcriptional control in these early-branching eukaryotes (10, 14, 15). Using the *L. donovani* LD1S experimental strain and conducting *in vitro* evolutionary experiments, we demonstrated the highly dynamic, reversible and reproducible nature of parasite karyotypic changes, and correlated chromosome amplification to fitness gains in culture (13). Using recent clinical isolates of *L. donovani*, we demonstrated that such karyotypic changes were strain-specific (12), suggesting a potential link between the genetic background of the parasite and its karyotype plasticity (12, 16). Despite the potential relevance of genomic adaptation in shaping the parasite pathogenic potential, only little is known about the dynamics of gene and chromosome CNVs in *Leishmania* field isolates while they evolve to adapt to new environments. Here we address this important open question by comparing the genomes of ten clinical isolates belonging to three different *Leishmania* complexes (*L. donovani, L. major, L. tropica*) from eight geographical regions. Read depth analysis revealed gene and chromosome CNV as potential drivers of long-term and short-term adaptation, respectively. Isolates during early and later stages of culture adaptation showed reproducible karyotypic changes for a given strain, providing strong evidence that chromosomal amplification is under positive selection. Significantly, these changes occurred in an individualized manner in even highly related strains, thus implicating for the first time environment-independent intrinsic genetic factors affecting *Leishmania* karyotypic adaptation.

Material and Methods

***Leishmania* parasite isolation and culture.** Ten *Leishmania* strains belonging to the *L. tropica*, *L. major* and *L. donovani* complexes of eight different geographical areas were isolated from infected patients, dogs or hamster (**Table S1**). Some strains were cryopreserved in liquid nitrogen prior to culture adaptation until used for this study (**Table S1**). *Leishmania* isolates were first stabilized *in vitro* in media that were optimized in the various LeiSHield partner laboratories ('Stabilization medium', **Table S2**), prior to expansion in classical RPMI culture medium for a defined number of passages ('Expansion medium'). Seven strains belonging to the *L. donovani* complex were selected for the comparison of intra-species evolvability in culture. These include the four *L. infantum* strains Linf_ZK27 from Tunisia, Linf_LLM56 and Linf_LLM45 from Spain, and Lin_02A from Brazil (voucher to asses this sample at Coleção de Leishmania do Instituto Oswaldo Cruz (CLIOC): IOCL3598), and the three *L. donovani* strains Ldo_BPK26 from India, Ldo_LTB from Sudan, and Ldo_CH33 from Cyprus. The latter strain belongs to the *L. donovani* MON-37 zymodeme (17-19) and multilocus microsatellite typing (MLMT) analysis has positioned it in a novel *L. donovani sensulato* (s.l.) group (20). Our analysis further included two *L. major* strains (Lmj_1948 from Tunisia, Lmj_A445 from Algeria) and one *L. tropica* strain (Ltr_16 from Morocco) (**Table S1**). Genotyping methodologies were applied to confirm species identity of the strains used in this work (**Table S1**). Standardized procedures for DNA sample preparation and cell (sub)-culturing were used in all partner laboratories (**Table S2**). Promastigotes from early cell culture (passage 2 of growth in Expansion medium, referred to as early passage samples, EP) and derived parasites maintained in culture for three more *in vitro* passages (EP+3) were processed for whole-genome sequencing (WGS) using parasites from late logarithmic growth phase. While different *Leishmania* strains can show differences in terms of generation time and can reach different population densities, we previously estimated that a single passage in culture corresponds to ca. 10 generations (13). To determine reproducibility of *in vitro* genome evolution, duplicate EP+3 samples (EP+3.1 and EP+3.2) were generated for the Linf_ZK27, Lmj_1948, Lmj_A445, Ldo_BPK26 and Ltr_16 strains (**Figure S1**). Culture conditions and time in culture for the 25 samples are detailed in **Table S2**.

Nucleic acid extraction, sample preparation and sequencing analysis. Procedures for DNA sample preparation and quality control were standardized using common protocols. Briefly, DNA extraction was performed using DNeasy blood and tissue kits from Qiagen according to manufacturer instructions. Nucleic acid concentrations were measured with Qubit and the DNA quality was evaluated on agarose gel. Between 2 to 5µg of DNA were used for sequencing. The following samples showed low DNA amounts and were thus PCR amplified before sequencing: Ldo_LTB_EP (five cycles), Ldo_LTB_EP+3 (five cycles), Linf_02A_EP (ten cycles), Linf_02A_EP+3 (five cycles). No PCR amplification was performed for the other samples.

Whole genome, short-insert, paired-end libraries were prepared for each sample. Samples Ltr_16_EP, Ltr_16_EP+3.1, Ltr_16_EP+3.2, Ldo_BPK26_EP, Ldo_BPK26_EP+3.1, Ldo_BPK26_EP+3.2, Lmj_A445_EP, Lmj_A445_EP+3.1, Lmj_A445_EP+3.2 were sequenced by the Biomics sequencing platform (https://research.pasteur.fr/en/team/biomics/) with Hiseq 2500 rapid runs, resulting in 2×108bp reads using the NEXTflex PCR-Free kit. All other samples were sequenced with the KAPA Hyper Prep Kit (Kapa Biosystems) at Centro Nacional de Análisis Genómico (CNAG, http://www.cnag.crg.eu/) using the TruSeq SBS Kit v3-HS (Illumina Inc.). Multiplex sequencing was performed according to standard Illumina procedures, using a HiSeq2000 flowcell v3 generating 2×101bp paired-end reads. Reads were deposited in the Sequence Read Archive database (SRA) database (21) and are publicly available under the accession number SRP126578.

Read alignment. Gene annotations and reference genomes of *L.major* Friedlin and *L. infantum* JPCM5 were downloaded from the Sanger FTP server (22) (URL ftp://ftp.sanger.ac.uk/pub/project/pathogens/gff3/CURRENT/) on 09/05/2017, whereas PacBio *L. donovani* LDBPK assembly and annotations were downloaded on 02/05/2017 (URL ftp://ftp.sanger.ac.uk/pub/project/pathogens/Leishmania/donovani/LdBPKPAC2016beta). The reads were aligned to the reference genomes with *BWA mem* (version 0.7.12) (23, 24) with the flag -M to mark shorter split hits as secondary. *Samtools fixmate*, *sort*, and *index* (25) (version 1.3) were used to process the alignment files and turn them into bam format. *RealignerTargetCreator* and *IndelRealigner* from the *GATK* suite (26-28) were run to homogenize indels. Eventually, PCR and optical duplicates were labeled with *Picard MarkDuplicates* (https://broadinstitute.github.io/picard/, version 1.94 (1484)) using the option 'VALIDATION_STRINGENCY=LENIENT'. While the reads were aligned against full assemblies, including unsorted contigs, just the canonical 36 chromosomes were considered for downstream analyses of ploidy estimation and copy number alterations. This filter was necessary because of the high content of repetitive elements and the absence of comparable and high quality annotations in the contigs. Given that the *L. tropica* reference genome is still unfinished, the sample Ltr_16 was aligned against the *L. major* Friedlin genome. Overall, starting from a total of 1,011,803,806 short reads, 952,093,114 were successfully aligned to the respective reference genomes (**Table S3**). *Picard CollectAlignmentSummaryMetrics* was used to estimate sequencing and mapping statistics.

Comparative genome analysis. Whole genome sequencing data from the EP *Leishmania* isolates were processed with *Trimmomatic* (29) (version 0.35) to remove low quality bases (options LEADING:3 TRAILING:3 SLIDINGWINDOW:4:15) and adapter contaminations (ILLUMINACLIP option, with values 2:30:12:1:true). Reads that were shorter than 36 bases after filtering were discarded (option MINLEN:36). The trimmed reads were assembled with *SPAdes* (30) (version 3.7.0) with option 'careful'. The resulting contigs were used to estimate the average nucleotide identity (ANI) with *dnadiff* part of *MUMmer* system (31) (version 3.23). The analysis included the reference genomes of *L. donovani, L. infantum* and *L. major* that were retrieved from the Sanger database (see above), and reference genomes of *L. braziliensis, L. mexicana*, and *L. panamensis* that were retrieved from ENSEMBL Protists release 29 (32). The ANI values were converted to a matrix of distances, which in turn were used for principal component analysis (PCA) and hierarchical clustering (R hclust function, https://www.r-project.org/).

Chromosome sequencing coverage. For each read alignment file, *Samtools view* (version 1.3) and *BEDTools genomecov* (33) (version 2.25.0) were used to measure the sequencing depth of each nucleotide. *Samtools* was run with options '-q 50 -F 1028' to discard reads with low map quality score or potential duplicates, while *BEDTools genomecov* was run with options '-d -split'. Nucleotide coverage was normalized by the median genomic coverage.

The chromosome sequencing coverage was used to evaluate aneuploidy between EP and EP+3 samples. For each sample and for each chromosome the median sequencing coverage was computed for contiguous windows of 2,500 bases. For those strains where two EP+3 samples were available, the mean of EP+3.1 and EP+3.2 was used to calculate the statistical significance of amplification compared to EP. The distribution of the median window coverage in EP and EP+3 were compared with 1-way ANOVA. To have an estimate of the chromosome copy number differences, the window coverage was further normalized by chromosome 19 median coverage and multiplied by two. For each chromosome the median values in EP and EP+3 were compared. Both the ANOVA P-values and the chromosome somy comparisons are reported in **Table S4.**

Gene sequencing coverage. *Samtools view* (version 1.3) and *BEDTools coverage* (version 2.25.0) were used to measure the mean sequencing depth of every annotated gene and were run respectively with options '-q 50 -F 1028' and '-d -split'. Possible intragenic gap regions were excluded from the calculation of the mean. Then the mean coverage of each gene was normalized by the median coverage of its chromosome. To account for GC content sequencing bias, the coverage values were corrected using a LOESS regression with a 5-fold cross validation to optimize the model span parameter. Genes supported by reads with a mean mapping quality (MAPQ) score < 50 were filtered.

To enable CNV analysis of gene arrays and genes sharing high sequence identity we clustered the nucleotide sequence of the annotated genes into groups with *cd-hit* (34) (version 4.6). We used the length difference cutoff option '-s 0.9'. Then we realigned the clusters with MAFFT (35) and used *T-Coffee seq_reformat* (36) to select a representative gene per cluster (RefGene) showing the highest average sequence similarity with the other cluster members. If two genes had the same average similarity then the shortest was chosen. We used *bwa* to build a database containing only the sequences of RefGene, adding +/- 50 base pairs of the 5' and 3' ends to ease the read alignment and the quantification of small RefGenes. We realigned EP samples against this database using *bwa mem* with the option '-M'. We then quantified the RefGene mean coverage (without considering the +/-50 base pairs extension) with *Samtools view* and *BEDTools coverage* using options '-F 1028' and '-d -split', respectively. Values were normalized by the median coverage of the RefGene's chromosome. Gene groups composed by members located on different chromosomes were negligible and discarded.

Genome binning. The reference genomes were divided into contiguous windows of a fixed length, and the sequencing coverage of each window was evaluated and compared across different samples. A window length of 300 bases was used for the shown scatter plots assessing genome-wide CNVs. Both the mean sequencing coverage normalized by the median chromosome coverage and the mean read MAPQ value were computed. To account for GC content sequencing bias, the coverage values were corrected using a LOESS regression with a 5-fold cross validation to optimize the model span parameter. The windows with MAPQ score below 50 in either EP or EP+3.1 were discarded. Poorly supported windows with median or mean sequencing depth smaller than one tenth of the median chromosome coverage both in EP and EP+3.1 were also discarded. The windows with EP+3/EP coverage ratio outside the axes limits were placed on the edge (value of 3). In the genome browser tracks the repeat elements and low complexity regions were predicted with *RepeatMasker* (RepeatModeler software: Smit, AFA, Hubley, R. *RepeatModeler Open-1.0*. 2008-2015. 2008. Available: http://www.repeatmasker.org) (version 4.0.6) using options '-e crossmatch -gff -xsmall -s' in combination with *Repbase* (37) to identify *Leishmania*-specific and ancestral repeats.

A window length of 2,000 bases was used for the shown circos plots assessing chromosome amplification. Mean sequencing coverage and mean MAPQ score of the reads aligning to that window were reported. The histogram function of *Circos* (version 0.68-1, (38)) was used to visualize the coverage of the windows, using a cut off of 3. Windows with mean MAPQ score below 50 or overlapping genomic gaps of over 1kb were assigned a sequencing coverage of 1.

Single nucleotide variants analysis. To call single nucleotide variants (SNVs) we used *Freebayes* (39) (version v1.0.1-2-g0cb2697) with options '--no-indels --no-mnps --no-complex --read-mismatch-limit 3 --read-snp-limit 3 --hwe-priors-off --binomial-obs-priors-off --allele-balance-priors-off --min-alternate-fraction 0.05 --min-base-quality 5 --min-mapping-quality 50 --min-alternate-count 2 --pooled-continuous'. The output was filtered to retain the positions with just one alternate allele with a minimum frequency of 0.9, and a minimum mean mapping quality of 20 for the reads supporting the reference or the alternative allele. SNVs mapping inside homopolymers (i.e. simple repeats of the same nucleotide) were filtered using a more stringent parameter, requiring at least 20 reads supporting the variant. The homopolymers were defined as the DNA region spanning +/- 5 bases from the SNV, with over 40% of identical nucleotides. We discarded SNVs with sequencing coverage above or below four median absolute deviations (MADs). The predicted SNVs are reported in **Table S5**.

Analysis of structural variants. *DELLY* (40) (version 0.6.7) was run with option '-q 50' to predict balanced structural variations, including translocations and inversion. To reduce false predictions, the *DELLY* output was additionally filtered removing structural variants overlapping for more than 50% of their size with either assembly gaps or repetitive elements. Predictions mapping within 10kb from the telomeric ends were removed to reduce false positive results caused by possible misassembled regions close to the chromosome ends. Signals showing *DELLY* paired-end support of the structural variant (PE) or the high-quality variant pairs score (DV) inferior to 20 were removed, as well as signals showing high-quality variant pairs inferior to 20. The predicted structural variants were represented with *Circos*.

Synteny analysis. The synteny analysis was performed with *SyntView* (41), a software package originally designed to compare microbial genomes. The tool was adapted to browse interactively the genome of four *Leishmania* reference genomes and explore their syntenic relation: *L. infantum* JPCM5, *L. donovani* PBQ7IC8, *L. major* Friedlin, *L. donovani* BPK282A1. This new tool hosting *Leishmania* syntenic data is publicly available at http://genopole.pasteur.fr/SynTView/flash/Leishmania/SynWebLinfantum.html**.**

Supplementary tables availability. All supplementary tables are publicly available at: https://gitlab.pasteur.fr/gbussott/Leishmania_genome_dynamics_during_environmental_adaptation_reveals_strain_specific_differences/.

Accession number. Reads were deposited in the Sequence Read Archive database (SRA) database and are publicly available under the accession number SRP126578.

Results

Analyzing the evolutionary relationship among *Leishmania* strains. Ten *Leishmania* strains belonging to the *L. tropica*, *L. major* or *L. donovani* complexes were obtained from different sources and regions (see methods, see **Table S1**) and parasites from early and later culture passages (designated EP and EP+3 respectively, **Figure S1**, **Table S2**) were subjected to sequencing analysis.

We first used the EP sequence information to confirm species determination and to characterize strain-specific genetic variations that may inform on mechanisms of adaptation. PCA and clustering analyses based on the average nucleotide identity (ANI) among strains confirmed the molecular determination of the various *Leishmania* species (**Figure S2 A** and **B**), with *L. infantum* and *L. donovani* or *L. major* and *L. tropica* grouping together, respectively. Ldo_CH33 grouped with other *L. donovani* strains, thus confirming previous zymodeme analysis (17-19). Based on branch length that correlates with genetic distance, the *L. infantum* isolates Linf_ZK27, Linf_LLM56, Linf_LLM45 and Linf_02A are highly related as was expected by their common epidemiological classification as MON-1 (**Table S1**).

Comparing the repertoire of high frequency SNVs (>90%) across the *L. infantum* isolates (**Figure 1A**) confirmed the very close relationship among these samples despite their geographic distance, with less than 600 strain-specific SNVs observed for a given isolate. The majority of SNVs shows a low frequency (data not shown), suggesting that nucleotide variants may not be under strong selection in this species. In contrast, the *L. donovani* strains are evolutionarily more distant as judged by the presence of over 40,000 strain-specific SNVs, with high frequency SNVs likely being associated with defined haplotypes that may be under selection as previously suggested (13, 42), or may be the result of geographic separation and genetic drift (**Figure 1B**).

Finally, the SNV analysis revealed the close genetic relationship between the Tunisian and Algerian *L. major* samples with 36,726 SNVs shared between the strains compared to the reference genome (**Figure 1C**). The massive amount of SNVs identified in *L. tropica* confirmed the large evolutionary distance to *L. major* strains observed by PCA and the clustering analyses (**Figure S2**). Differences in the evolutionary relationship were further supported by the absence of inversions or translocations in the *L. major* and *L. infantum* strains compared to the corresponding reference genomes, and the presence of translocations in the Cypriot Ldo_CH33 strain and the Sudanese *L. donovani* strain Ldo_LTB (**Figure 1D**, and **Table S6**), revealing a potential role of these structural genome variation in *L. donovani* adaptation.

Strains-specific gene copy number variations. Cross-comparing read depth among the EP samples revealed important intra-species variations in copy number for single- and multi-copy genes (**Table S7**, see methods). Plotting the gene coverage values for the three *L. infantum* isolates, or the three *L. donovani* isolates, or the two *L. major* isolates together with the *L. tropica* sample, resulted in strong, confined signals at the center of the ternary plots that correspond to genes with equal copy number and thus a 33% distribution across the three axes (**Figure 2**, left panels). Compared to the different reference genomes, we observed important, strain-specific differences in gene copy number that are visualized on these plots by shifts of the signals out of the centre. Overall, using a cut off of 0.5 increase or decrease in normalized read depth of 1 (corresponding to the copy number per haploid genome) we observed 67, 152 and 119 strain-specific amplifications for respectively *L. infantum, L. donovani*, and *L. major* (**Table S8**). A selection of annotated genes is shown in

Tables 1 and **2** (for the full panel see **Table S8**) and prominent examples are represented on the right panels of **Figure 2**.

In *L. infantum* we observed (i) a 2.94-fold amplification in Linf_LLM56 of LinJ.30.2990 encoding for a glyceraldehyde 3-phosphate dehydrogenase, (ii) a cluster of seven genes (Linj.29.0050 - Linj.29.0110) located in a ~23 kb region delimited by SIDER repetitive elements that showed a two-fold amplification in Linf_ZK27, and (iii) the amplification (up to 32-fold) of the GP63 leishmanolysin cluster (LinJ.10.0490 - LinJ.10.0530) in Linf_02A. For *L. donovani* we identified (i) a 48-fold amplification specific to Ldo_LTB of a cluster of ten genes (LdBPK_350056400 - LdBPK_350057300), which includes a biopterin transporter, an RNAse-P, an RNA pseudouridylate synthase and a putative ribosomal L37e protein, (ii) an up to 26-fold amplification in Ldo_BPK26 of a putative amastin surface glycoprotein (LdBPK_340024100), and (iii) the deletion in Ldo_CH33 and partial depletion in Ldo_LTB of a putative amastin-like surface protein (LdBPK_340015500). Finally, as expected from their phylogenetic relationship, important differences were observed in gene CNVs between the *L. tropica* and *L. major* strains, including (i) an amplification on chromosome 35 in both Lmj_1948 and Lmj_A445 (respectively of 3.51 and 2.63-fold), spanning a hypothetical protein (LmjF.35.0250) and the 5’ of a putative GTP-ase activating protein (LmjF.35.0260), (ii) an up to 6-fold amplification in Ltr_16 of a putative KU80 protein (LmjF.30.0340) flanked by SIDER2 elements, and (iii) an Lmj_A445-specific amplification of a snoRNA cluster on chromosome 26.

Together these results suggest that gene CNVs may drive or be the result of adaptation of otherwise highly related *Leishmania* field isolates, causing phenotypic differences with respect to stress resistance, nutrition, and infectivity as judged by gene CNVs observed in heat shock proteins, transporters, and known virulence factors (see **Tables**

1 and **2**). Thus gene CNV seems to shape the parasite genome and likely its pathogenic potential in the field through positive (amplification) and purifying (deletion) selection, potentially driving long-term adaptation to ecological constraints of local transmission cycles.

Dynamic karyotype changes during extended growth in culture. We next assessed structural genomic variations that may drive short-term environmental adaptation comparing EP and EP+3 samples that evolved *in vitro* during culture adaptation. WGS and read depth analysis revealed important karyotype differences between the two *in vitro* passages of a given strain (intra-strain variation) and among different strains (inter-strain variation). Aside an intra-chromosomal duplication at both EP and EP+3 observed in Ldo_LTB spanning nearly half of chromosome 27 (453.410 bases) affecting 113 genes, changes in read depth were homogenous across all chromosomes thus revealing frequent aneuploidy (**Figure S3**). Linf_ZK27 and Ldo_LTB displayed the most stable karyotypes between EP and EP+3. As judged by read depth values corresponding to integer or intermediate chromosome copy number values, full or mosaic aneuploidy was observed for four (chromosome 6, 9, 31, 35 for Linf_ZK27) and six chromosomes (chromosome 13, 15, 20, 23, 31, 33 for Ldo_LTB), which were established at EP and maintained at EP+3 (**Figure 3** and **Table S4**). All other isolates showed higher intra-strain karyotype instability with both gain and loss of chromosomes observed between EP and EP+3. Linf_02A represented the most extreme example showing significant changes in read depth for twenty-one chromosomes (**Figure 3** and **Table S4**) and five chromosomes with a somy score difference higher than 0.5 compared to the disomic state corresponding to 2 (**Table S4**, see methods). Overall, chromosomes 20 and 23 showed the highest propensity for amplification between EP and EP+3, with different ploidy levels (mosaic aneuploidy, trisomy, tetrasomy) observed in respectively nineteen and fifteen samples out of twenty-five, suggesting that amplification of these chromosomes may provide fitness advantage during culture adaptation for most of the strains analyzed in our study.

With the exception of the previously reported, stable aneuploidy for chromosome 31 (10), the dynamics of the observed karyotypic changes are substantially different among all isolates. It is interesting to speculate that this heterogeneity reflects individualized solutions driving fitness gains *in vitro*. While differences in culture conditions certainly account for some of the observed karyotypic variability, the comparison of two closely related Spanish *L. infantum* isolates Linf_LLM45 and Linf_LLM56 reveals a culture-independent component implicated in genomic adaptation. Both isolates were adapted to culture at the same time under the same conditions, yet showed important differences in karyotype dynamics, with only Linf_LLM56 demonstrating changes in somy levels at EP+3 (**Figure 3** and **Table S4**). These strains are genotypically identical (zymodeme MON-1) (**Table S1**) and are genetically closely related with an average nucleotide identity of over 99.95%, suggesting that minor genetic differences may have important impact on *Leishmania* karyotypic adaptation to a given environment. Aside SNVs (see **Figure 1**), the difference in karyotype dynamics may be linked to gene CNVs observed between the Linf_LLM45 and Linf_LLM56, which affected genes implicated for example in protein translation, protein folding, or protein turnover (**Table 3**).

Despite this remarkable plasticity of the *Leishmania* karyotype, we observed that changes in chromosome number are highly reproducible in duplicate EP+3 samples that were derived for *L. major* (Lmj_1948 and Lmj_A445), *L. infantum* (Linf_ZK27), *L. donovani* (Ldo_BPK26) and *L. tropica* (Ltr_16) (**Figure 3**). Thus, even though karyotypic fluctuations may arise in a stochastic manner - either in the host or during culture adaptation, our data demonstrate that beneficial karyotypes are under strong selection during culture adaptation. Significantly, the SNV frequency profiles for EP and EP+3 were largely identical, ruling out the possibility that adaptation occurs through selection of sub-populations that would cause important shifts in SNV frequency distribution (data not shown). Together our results document the highly dynamic nature of karyotype management in *Leishmania* during environmental adaptation that is likely governed by complex interactions between external cues and intrinsic genetic differences.

Dynamic variations in gene copy number during *de novo* culture adaptation. Plotting genome-wide sequencing coverage of EP+3 against EP for all annotated genes resulted in a largely diagonal distribution, suggesting that there are no major CNVs between the two different passages (**Figure 4A**, **Figure S4**, **Table S9**). Overall, the majority of genes were scattered around a normalized coverage of 1 (corresponding to the copy number per haploid genome, see methods), suggesting that their copy number matches the one in the reference strains. We nevertheless observed a significant number of genes across all isolates that showed coverage either below 0.5 or above two-fold, independent of culture passage, thus revealing important differences between the isolates and their corresponding reference genomes. This analysis uncovered a significant increase in coverage at EP+3 for all chromosomes of strain Linf_02A (**Figure 4B, Table S9**), indicating some form of CNV that correlated with increased culture passage. In the following, we more closely investigated the structural basis of these culture-associated CNVs in Linf_02A.

Telomeric amplification. We partitioned the genome into contiguous windows and plotted the coverage at EP or EP+3 samples, as well as the ratio between EP+3 and EP. We observed a significant increase in read depth towards the telomeres in both EP and EP+3 for Lmj_1948, while coverage fluctuations in EP+3 were observed for Ltr_16, Lmj_A445, and Linf_02A, generating a repetitive pattern when plotting the entire genome (**Figure 5A**). The observed increase in read depth is not discrete but gradual, spanning from sub-telomeric regions to the telomeres and thus cannot be assigned to misannotation of the number of telomeric repeats in the reference genome (that should cause a discrete but not progressive increase in read depth at the telomeres only). The gradual increase in read depth supports the increased gene coverage and contributes to the shift in the chromosome coverage distribution we observed for strain Linf_02A at EP+3 (**Figure 4B** and **Figure 3**). We found the gradual increase in read depth to be disrupted for chromosomes 7 and 13 by regions with lower read depth (**Figure 5B** and **Figure S5**). According to our model, these genomic elements should not be part of sub-telomeric regions and thus either reflect a strain-specific recombination event or misassembly of the *L. infantum* reference genome. Synteny analysis among available reference genomes showed that the disruptive sequence elements observed in Linf_02A show sub-telomeric localization in *L. major* and the novel PacBio generated LdBPK genome (12), revealing misassembly of these regions in the current *L. infantum* and the previous *L. donovani* reference genomes (**Figure 5C**). This 'diagnostic' value of our result confirms that telomeric amplification is not a technical artefact, but represents a non-conventional mechanism of telomeric amplification in *Leishmania* that may be similar to those described in other organisms (43).

Discussion

Drawing from newly generated genome sequences of *Leishmania* clinical isolates and conducting longitudinal studies *in vitro* we demonstrate the existence of strain-specific gene copy number variations that may drive long-term and short-term evolutionary trajectories in *Leishmania*. We show that highly related *Leishmania* isolates that evolved in different regions are distinguished by both amplification and loss of genes linked to parasite infectivity, such as GP63 or amastins. The fixation of these genetic alterations may not be random but could potentially be the result of positive or purifying selection processes that are functional and adapt parasite fitness to a given ecology or transmission cycle. Identification of such genomic alterations that are under selection by the host can directly inform on genetic loci that are clinically relevant. The corresponding genes may be prioritized for functional genetic analysis (notably those genes that are not annotated) as they may play important roles in virulence and may qualify as biomarkers with diagnostic or prognostic value.

Monitoring genetic fluctuations using *de novo* culture as a proxy for short-term environmental adaptation revealed two forms of dynamic genomic changes. First, as judged by the establishment of reproducible aneuploidy profiles in duplicate cultures of a given strain, chromosomal amplification is the result of selection rather than random genetic drift. This result corroborates our previous observations in the *L. donovani* experimental strain LD1S, where spontaneous karyotypic fluctuations generate genotypically and phenotypically diverse mosaic populations that are substrate for evolutionary adaptation and fitness gain in response to environmental change (13). Whether chromosomal amplification occurs de novo during culture adaptation or reflect an initial diversity in each clinical isolate remains to be established, even though the karyotype mosaicism we previously observed in situ in *L. donovani* infected hamster spleen and liver favours the latter explanation (13).

Second, we uncovered a novel mechanism of telomeric amplification in three different *Leishmania* species (*L. major, L. tropica* and *L. infantum*) as revealed by a progressive increasing in sequencing read depth towards the chromosome ends. Non-classical mechanisms of telomere maintenance have been documented in a variety of eukaryotes, including (i) rolling circle replication in *Kluyveromyces lactis*, implicating extra-chromosomal circular templates (44), (ii) break-induced replication in *Saccharomyces cerevisiae* involving recombination between tracts of telomeric repeats (45), or (iii) telomeric loop formation first observed in human and mouse cells, where a telomere 3' end loops back to invade the duplex part of the same telomere and anneal with complementary telomeric repeat sequence (43). Our observation of a gradual increase in read depth from large sub-telomeric regions towards the chromosome ends is compatible with rolling circle replication, considering the propensity of *Leishmania* to extra-chromosomal amplification (9), the absence of telomeric repeats in sub-telomeric regions in Linf_02A that would allow for telomeric loop formation (data not shown), and the presence of only very small telomeric loops of less than 1kb in the related pathogen *Trypanosoma brucei* (46). Given that bona fide amastigotes cannot be maintained or adapted to culture, our *in vitro* evolutionary experiments were conducted with insect-stage promastigotes that were directly derived from tissue-derived amastigotes. Thus, the various forms of genomic instability we observed in our system likely drive adaptation and fitness gain in the sand fly vector. While we previously documented the prevalence of chromosomal amplification in tissue amastigotes (13), the presence of telomeric amplification at this stage remains to be established.

Our comparative genomics approach further provided a powerful tool to reveal species- and strain-specific variations in genomic adaptation. Telomeric amplification was only seen in three of the ten isolates, and very different karyotypic solutions were observed even in closely related isolates under the same culture conditions, revealing the significance of environment-independent, intrinsic factors in genomic adaptation. Using the highly related Spanish isolates Linf_LLM56 and Linf_LLM45 as an example, various genetic determinants may be implicated. Both strains were obtained from the same area at a short time frame, suggesting a very recent common ancestor as confirmed by their genetic similarity. Nevertheless, they were isolated from two stray dogs and genetic differences of both mammalian and insect hosts during natural infection may have shaped the parasite genomes in different ways through genotype-genotype interactions, as observed for example in anopheline mosquitoes infected with *Plasmodium falciparum*, the causal agent of malaria (47). Given the intrinsic instability of the *Leishmania* karyotype we observed *in situ* during visceral infection in liver- and spleen-derived amastigotes (13), these interactions may establish a very different chromosomal stoichiometry among canine isolates, which then translates into the different karyotypic trajectories we observed during culture adaptation. Likewise, differences in the number of single-copy genes or CNVs in multi-copy gene arrays generated by intra- or extra-chromosomal amplification (9) may impact on the karyotypic profile, with gene amplification alleviating the need for chromosome duplication as previously suggested (10). Finally, we cannot rule out that individual SNVs in coding sequences or regulatory elements 5’ and 3’ UTRs may impact on genomic adaptation, a possibility that is supported by our previous observation of tissue-specific haplotype selection in the liver and spleen of *L. donovani* infected hamsters (13).

In conclusion, our results draw a complex picture of *Leishmania* genomic adaptation in the field and in culture that needs to be considered in epidemiological studies that correlate parasite phenotypic variability and disease outcome. Adaptation is highly individualized and results from a dynamic selection process acting on genetically heterogeneous parasite populations that thrive inside distinct and genetically equally heterogeneous hosts (e.g. insects, rodents, humans). For environmental adaptation, *Leishmania* can draw from a vast genetic landscape of spontaneous karyotypic fluctuations, stochastic gene amplifications, and nucleotide polymorphisms. Our comparison of highly related Spanish *L. infantum* isolates revealed that even small variations in sequence might result in important differences in karyotypic adaptation. Thus, closely related isolates evolving in the same epidemiological niche can attain similar levels of fitness in a highly pleotropic way using alternative genetic solutions (13). This form of pleiotropic adaptation is characteristic for pathogenic microbes that maintain genetic heterogeneity and thus evolvability despite strong selection. Our data indicates that *Leishmania* adopts a similar, polyclonal adaptation strategy, which may strongly limit the identification of biomarkers with broad clinical relevance across *Leishmania* species or even related *Leishmania* strains. Future efforts need to take this complexity into account and approach the epidemiology of *Leishmania* infection on an integrative level, considering genotype-genotype and environment-genotype interactions, and dissecting the population structure of individual isolates by single cell, direct tissue sequencing.

Acknowledgements

This study was supported by a seeding grant from the Institut Pasteur International Department to the LeiSHield consortium, the EU FP7 (Kaladrug-R, contract 222895), the Belgian Science Policy Office (TRIT, P7/41), the Department of Economy, Science and Innovation in Flanders (ITM-SOFIB) and the Flemish Fund for Scientific Research (G.0.B81.12) (J.C.D., F.D.).

References

1. Jun 2015. 5. A touch of Zen: post-translational regulation of the Leishmania stress response. Cell Microbiol, 17.632-638. http://eutils.ncbi.nlm.nih.gov/entrez/eutils/elink.fcgi?dbfrom=pubmed&amp;id=25801803&amp;retmode=ref&amp;cmd=prlinks.
2. Apr 30 1984. 4643. Identification of an infective stage of Leishmania promastigotes. Science, 223.1417-1419. http://eutils.ncbi.nlm.nih.gov/entrez/eutils/elink.fcgi?dbfrom=pubmed&amp;id=6701528&amp;retmode=ref&amp;cmd=prlinks.
3. 1994. The role of pH and temperature in the development of Leishmania parasites. Annu Rev Microbiol, 48.449-470. http://eutils.ncbi.nlm.nih.gov/entrez/eutils/elink.fcgi?dbfrom=pubmed&amp;id=7826014&amp;retmode=ref&amp;cmd=prlinks.
4. 2013. 11. Proteomic and genomic analyses of antimony resistant Leishmania infantum mutant. PLoS ONE, 8.e81899. http://eutils.ncbi.nlm.nih.gov/entrez/eutils/elink.fcgi?dbfrom=pubmed&amp;id=24312377&amp;retmode=ref&amp;cmd=prlinks.
5. Dec 2011. 12. Whole genome sequencing of multiple Leishmania donovani clinical isolates provides insights into population structure and mechanisms of drug resistance. Genome Res, 21.2143-2156. http://eutils.ncbi.nlm.nih.gov/entrez/eutils/elink.fcgi?dbfrom=pubmed&amp;id=22038251&amp;retmode=ref&amp;cmd=prlinks.
6. 2016. Plasticity of the Leishmania genome leading to gene copy number variations and drug resistance. F1000Res, 5.2350. http://eutils.ncbi.nlm.nih.gov/entrez/eutils/elink.fcgi?dbfrom=pubmed&amp;id=27703673&amp;retmode=ref&amp;cmd=prlinks.
7. May 2009. 5. Gene expression modulation is associated with gene amplification, supernumerary chromosomes and chromosome loss in antimony-resistant Leishmania infantum. Nucleic Acids Res, 37.1387-1399. http://eutils.ncbi.nlm.nih.gov/entrez/eutils/elink.fcgi?dbfrom=pubmed&amp;id=19129236&amp;retmode=ref&amp;cmd=prlinks.
8. May 2013. 1. Telomeric gene deletion and intrachromosomal amplification in antimony-resistant Leishmania. Mol Microbiol, 88.189-202. http://eutils.ncbi.nlm.nih.gov/entrez/eutils/elink.fcgi?dbfrom=pubmed&amp;id=23421749&amp;retmode=ref&amp;cmd=prlinks.
9. Jun 2014. 5. Genome-wide stochastic adaptive DNA amplification at direct and inverted DNA repeats in the parasite Leishmania. PLoS Biol, 12.e1001868. http://eutils.ncbi.nlm.nih.gov/entrez/eutils/elink.fcgi?dbfrom=pubmed&amp;id=24844805&amp;retmode=ref&amp;cmd=prlinks.
10. Dec 2011. 12. Chromosome and gene copy number variation allow major structural change between species and strains of Leishmania. Genome Res, 21.2129-2142. http://eutils.ncbi.nlm.nih.gov/entrez/eutils/elink.fcgi?dbfrom=pubmed&amp;id=22038252&amp;retmode=ref&amp;cmd=prlinks.
11. Jul 2014. 7. Genetic analysis of Leishmania donovani tropism using a naturally attenuated cutaneous strain. PLoS Pathog, 10.e1004244.

http://eutils.ncbi.nlm.nih.gov/entrez/eutils/elink.fcgi?dbfrom=pubmed&amp;id=24992200&amp;retmode=ref&amp;cmd=prlinks.

12. Jun 23 2017. 3. Modulation of Aneuploidy in Leishmania donovani during Adaptation to Different In Vitro and In Vivo Environments and Its Impact on Gene Expression. MBio, 8.http://eutils.ncbi.nlm.nih.gov/entrez/eutils/elink.fcgi?dbfrom=pubmed&amp;id=28536289&amp;retmode=ref&amp;cmd=prlinks.

13. Dec 2017. 12. Haplotype selection as an adaptive mechanism in the protozoan pathogen Leishmania donovani. Nat Ecol Evol, 1.1961-1969. http://eutils.ncbi.nlm.nih.gov/entrez/eutils/elink.fcgi?dbfrom=pubmed&amp;id=29109466&amp;retmode=ref&amp;cmd=prlinks.

14. Aug 2016. Gene expression in Kinetoplastids. Curr Opin Microbiol, 32.46-51. http://eutils.ncbi.nlm.nih.gov/entrez/eutils/elink.fcgi?dbfrom=pubmed&amp;id=27177350&amp;retmode=ref&amp;cmd=prlinks.

15. Jul 15 2005. 5733. The genome of the kinetoplastid parasite, Leishmania major. Science, 309.436-442. http://eutils.ncbi.nlm.nih.gov/entrez/eutils/elink.fcgi?dbfrom=pubmed&amp;id=16020728&amp;retmode=ref&amp;cmd=prlinks.

16. Apr 22 2016. Evolutionary genomics of epidemic visceral leishmaniasis in the Indian subcontinent. Elife, 5.http://eutils.ncbi.nlm.nih.gov/entrez/eutils/elink.fcgi?dbfrom=pubmed&amp;id=27003289&amp;retmode=ref&amp;cmd=prlinks.

17. Jun 2009. 6-7. The paraphyletic composition of Leishmania donovani zymodeme MON-37 revealed by multilocus microsatellite typing. Microbes Infect, 11.707-715. http://eutils.ncbi.nlm.nih.gov/entrez/eutils/elink.fcgi?dbfrom=pubmed&amp;id=19376262&amp;retmode=ref&amp;cmd=prlinks.

18. Feb 2008. 1. Leishmania donovani leishmaniasis in Cyprus. Lancet Infect Dis, 8.6-7. http://eutils.ncbi.nlm.nih.gov/entrez/eutils/elink.fcgi?dbfrom=pubmed&amp;id=18156082&amp;retmode=ref&amp;cmd=prlinks.

19. Mar 2009. 2. Leishmania donovani leishmaniasis in Cyprus. Lancet Infect Dis, 9.76-77. http://eutils.ncbi.nlm.nih.gov/entrez/eutils/elink.fcgi?dbfrom=pubmed&amp;id=19179221&amp;retmode=ref&amp;cmd=prlinks.

20. 2012. 2. Multilocus microsatellite typing (MLMT) of strains from Turkey and Cyprus reveals a novel monophyletic L. donovani sensu lato group. PLoS Negl Trop Dis, 6.e1507. http://eutils.ncbi.nlm.nih.gov/entrez/eutils/elink.fcgi?dbfrom=pubmed&amp;id=22348162&amp;retmode=ref&amp;cmd=prlinks.

21. Feb 2011. Database issue. The sequence read archive. Nucleic Acids Res, 39.D19-21. http://eutils.ncbi.nlm.nih.gov/entrez/eutils/elink.fcgi?dbfrom=pubmed&amp;id=21062823&amp;retmode=ref&amp;cmd=prlinks.

22. Feb 2012. Database issue. GeneDB--an annotation database for pathogens. Nucleic Acids Res, 40.D98-108. http://eutils.ncbi.nlm.nih.gov/entrez/eutils/elink.fcgi?dbfrom=pubmed&amp;id=22116062&amp;retmode=ref&amp;cmd=prlinks.

23. Dec 07 2013. Aligning sequence reads, clone sequences and assembly contigs with BWA-MEM. arXiv:13033997v1 [q-bioGN],

24. Jul 15 2009. 14. Fast and accurate short read alignment with Burrows-Wheeler transform. Bioinformatics, 25.1754-1760.

http://www.ncbi.nlm.nih.gov/entrez/query.fcgi?cmd=Retrieve&amp;db=PubMed&amp;dopt=Citation&amp;list_uids=19451168.

25. Aug 15 2009. 16. The Sequence Alignment/Map format and SAMtools. Bioinformatics, 25.2078-2079. http://eutils.ncbi.nlm.nih.gov/entrez/eutils/elink.fcgi?dbfrom=pubmed&amp;id=19505943&amp;retmode=ref&amp;cmd=prlinks.

26. Jun 2011. 5. A framework for variation discovery and genotyping using next-generation DNA sequencing data. Nat Genet, 43.491-498. http://eutils.ncbi.nlm.nih.gov/entrez/eutils/elink.fcgi?dbfrom=pubmed&amp;id=21478889&amp;retmode=ref&amp;cmd=prlinks.

27. Sep 2010. 9. The Genome Analysis Toolkit: a MapReduce framework for analyzing next-generation DNA sequencing data. Genome Res, 20.1297-1303. http://eutils.ncbi.nlm.nih.gov/entrez/eutils/elink.fcgi?dbfrom=pubmed&amp;id=20644199&amp;retmode=ref&amp;cmd=prlinks.

28. 2013. From FastQ data to high confidence variant calls: the Genome Analysis Toolkit best practices pipeline. Curr Protoc Bioinformatics, 43.11.10.1-33. http://eutils.ncbi.nlm.nih.gov/entrez/eutils/elink.fcgi?dbfrom=pubmed&amp;id=25431634&amp;retmode=ref&amp;cmd=prlinks.

29. Aug 01 2014. 15. Trimmomatic: a flexible trimmer for Illumina sequence data. Bioinformatics, 30.2114-2120. http://eutils.ncbi.nlm.nih.gov/entrez/eutils/elink.fcgi?dbfrom=pubmed&amp;id=24695404&amp;retmode=ref&amp;cmd=prlinks.

30. Jun 2012. 5. SPAdes: a new genome assembly algorithm and its applications to single-cell sequencing. J Comput Biol, 19.455-477. http://eutils.ncbi.nlm.nih.gov/entrez/eutils/elink.fcgi?dbfrom=pubmed&amp;id=22506599&amp;retmode=ref&amp;cmd=prlinks.

31. 2004. 2. Versatile and open software for comparing large genomes. Genome Biol, 5.R12. http://eutils.ncbi.nlm.nih.gov/entrez/eutils/elink.fcgi?dbfrom=pubmed&amp;id=14759262&amp;retmode=ref&amp;cmd=prlinks.

32. Feb 04 2016. D1. Ensembl Genomes 2016: more genomes, more complexity. Nucleic Acids Res, 44.D574-80. http://eutils.ncbi.nlm.nih.gov/entrez/eutils/elink.fcgi?dbfrom=pubmed&amp;id=26578574&amp;retmode=ref&amp;cmd=prlinks.

33. Apr 15 2010. 6. BEDTools: a flexible suite of utilities for comparing genomic features. Bioinformatics, 26.841-842. http://eutils.ncbi.nlm.nih.gov/entrez/eutils/elink.fcgi?dbfrom=pubmed&amp;id=20110278&amp;retmode=ref&amp;cmd=prlinks.

34. Jul 01 2006. 13. Cd-hit: a fast program for clustering and comparing large sets of protein or nucleotide sequences. Bioinformatics, 22.1658-1659. http://eutils.ncbi.nlm.nih.gov/entrez/eutils/elink.fcgi?dbfrom=pubmed&amp;id=16731699&amp;retmode=ref&amp;cmd=prlinks.

35. 2005. 2. MAFFT version 5: improvement in accuracy of multiple sequence alignment. Nucleic Acids Res, 33.511-518. http://eutils.ncbi.nlm.nih.gov/entrez/eutils/elink.fcgi?dbfrom=pubmed&amp;id=15661851&amp;retmode=ref&amp;cmd=prlinks.

36. Sep 08 2000. 1. T-Coffee: A novel method for fast and accurate multiple sequence alignment. J Mol Biol, 302.205-217. http://www.ncbi.nlm.nih.gov/entrez/query.fcgi?cmd=Retrieve&amp;db=PubMed&amp;dopt=Citation&amp;list_uids=10964570.

37. 2005. 1-4. Repbase Update, a database of eukaryotic repetitive elements. Cytogenet Genome Res, 110.462-467. http://eutils.ncbi.nlm.nih.gov/entrez/eutils/elink.fcgi?dbfrom=pubmed&amp;id=16093699&amp;retmode=ref&amp;cmd=prlinks.

38. Sep 2009. 9. Circos: an information aesthetic for comparative genomics. Genome Res, 19.1639-1645. http://eutils.ncbi.nlm.nih.gov/entrez/eutils/elink.fcgi?dbfrom=pubmed&amp;id=19541911&amp;retmode=ref&amp;cmd=prlinks.

39. Jul 20 2012. Haplotype-based variant detection from short-read sequencing. arXiv preprint arXiv:12073907 [q-bioGN],

40. Sep 15 2012. 18. DELLY: structural variant discovery by integrated paired-end and split-read analysis. Bioinformatics, 28.i333-i339. http://eutils.ncbi.nlm.nih.gov/entrez/eutils/elink.fcgi?dbfrom=pubmed&amp;id=22962449&amp;retmode=ref&amp;cmd=prlinks.

41. Sep 22 2013. SynTView - an interactive multi-view genome browser for next-generation comparative microorganism genomics. BMC Bioinformatics, 14.277. http://eutils.ncbi.nlm.nih.gov/entrez/eutils/elink.fcgi?dbfrom=pubmed&amp;id=24053737&amp;retmode=ref&amp;cmd=prlinks.

42. Feb 2018. 1. Genome wide comparison of Ethiopian Leishmania donovani strains reveals differences potentially related to parasite survival. PLoS Genet, 14.e1007133. http://eutils.ncbi.nlm.nih.gov/entrez/eutils/elink.fcgi?dbfrom=pubmed&amp;id=29315303&amp;retmode=ref&amp;cmd=prlinks.

43. May 2004. 4. T-loops and the origin of telomeres. Nat Rev Mol Cell Biol, 5.323-329. http://eutils.ncbi.nlm.nih.gov/entrez/eutils/elink.fcgi?dbfrom=pubmed&amp;id=15071557&amp;retmode=ref&amp;cmd=prlinks.

44. Jul 2002. 13. Recombinational telomere elongation promoted by DNA circles. Mol Cell Biol, 22.4512-4521. http://eutils.ncbi.nlm.nih.gov/entrez/eutils/elink.fcgi?dbfrom=pubmed&amp;id=12052861&amp;retmode=ref&amp;cmd=prlinks.

45. May 2000. 4. Recombination in telomere-length maintenance. Trends Biochem Sci, 25.200-204. http://eutils.ncbi.nlm.nih.gov/entrez/eutils/elink.fcgi?dbfrom=pubmed&amp;id=10754555&amp;retmode=ref&amp;cmd=prlinks.

46. Mar 01 2001. 3. t-loops at trypanosome telomeres. EMBO J, 20.579-588. http://eutils.ncbi.nlm.nih.gov/entrez/eutils/elink.fcgi?dbfrom=pubmed&amp;id=11157764&amp;retmode=ref&amp;cmd=prlinks.

47. Feb 11 2005. Host genotype by parasite genotype interactions underlying the resistance of anopheline mosquitoes to Plasmodium falciparum. Malar J, 4.3. http://eutils.ncbi.nlm.nih.gov/entrez/eutils/elink.fcgi?dbfrom=pubmed&amp;id=15644136&amp;retmode=ref&amp;cmd=prlinks.

48. Jul 08 2016. W1. deepTools2: a next generation web server for deep-sequencing data analysis. Nucleic Acids Res, 44.W160-5. http://eutils.ncbi.nlm.nih.gov/entrez/eutils/elink.fcgi?dbfrom=pubmed&amp;id=27079975&amp;retmode=ref&amp;cmd=prlinks.

Legends

Figure 1: SNVs and translocations with respect to the reference genomes. Venn diagrams showing the number of unique and shared SNVs among three *L. infantum* strains **(A)**, three *L. donovani* strains **(B)** and two *L. major* strains together with a *L. tropica* strain **(C)**. **(D)** *Circos* representation of genomic translocations in samples Ldo_CH33 and Ldo_LTB compared to the corresponding *L. donovani* reference genome. Connecting lines represent translocations events. Black and red lines demonstrate respectively Ldo_CH33 and Ldo_LTB specific translocations. Blue lines show translocations common in both stains. No inversions were detected using the filtering settings indicated in the methods section. Black, chromosomes; red, genes mapping on the positive strand; green, genes mapping on the negative strand.

Figure 2: Inter-strain gene CNV. (A – C) Ternary plots showing for each gene the relative abundance in the three considered strains (left panels). The axes report the fraction of the normalized gene coverage in the three strains with each given point adding up to 100. Black dots represent unique genes, whereas red dots indicate genes representing gene families. The comparison of three *L. infantum* strains **(A)**, three *L. donovani* strains **(B)** and two *L. major* strains together with a *L. tropica* strain **(C)** are shown. The right panels show examples of detected gene copy number variations (CNVs). From top to the bottom the tracks represent the sequencing depth measured in the three strains, the gene annotations and the predicted repetitive elements. Coverage tracks were produced with *bamCoverage* from the *deepTools* suit (48) (version 2.4.2) ignoring duplicated reads. RPKM normalization was applied to render the coverage comparable across samples.

Figure 3: Chromosome ploidy analysis. Box plots representing the normalized sequencing coverage distributions for each chromosome for the strains indicated. The lower and upper edges of the box show respectively the lower quartile (i.e. 25% of nucleotides with normalized coverage below that value) and upper quartile (i.e. 25% of nucleotides with normalized coverage above that value). The whiskers show maximum and minimum coverage values excluding outliers. Outliers are not shown to ease plot readability. Box sizes reflect coverage dispersion that can be affected by sample sequencing depth, chromosomal ploidy, intra-chromosomal copy number alterations, assembly gaps or repetitive regions. The increased box size visible in chromosome 27 of sample Ldo_LTB is caused by a large sub-chromosomal amplification (see **Figure S3**). In *L. donovani*, *L. major* or *L. tropica* samples, the presence of large gaps or repetitive regions inflate the box size for chromosomes 2, 8 and 12. Green, early passage EP; orange, EP+3.1 replicate; purple, EP+3.2 replicate.

Figure 4: Gene copy number variation (CNV) in culture adaptation. (A) Genome-wide scatter plot showing Log10 gene coverage of EP and EP+3 samples. Dots represent all genes annotated in the respective reference assemblies. **(B)** Chromosome-specific scatter plots of gene CNV between EP+3 versus EP. Only selected chromosomes are shown and the full panel is available in **Figure S4**. The red diagonal lines indicate the bisectors. The gray dashed horizontal lines mark a coverage value of 1. The axes' maximum and minimum values were adjusted to the most extreme values for each individual plot to avoid logarithmic compression. For both **(A)** and **(B)** the EP+3.1 replicate was used, except for Lmj_A445 for which EP+3.2 replicate was utilized.

Figure 5: Sub-telomeric amplification. (A) Genome-wide coverage ratios (y-axes) between EP and EP+3 of the indicated samples and their respective reference genomes (left and middle panels) or between EP+3/EP (right panels) are shown. The EP+3 coverage refers to the EP+3.1 replicate except for Lmj_A445 for which EP+3.2 replicate coverage was used. The x-axis reports the position of the genomic windows along the chromosomes. Dots represent genomic windows of 300 bases. In each panel the 36 *Leishmania* chromosomes are shown in sequential order. To ease the visualization, all scores > 3 were assigned to a value of 3. **(B)** The EP+3/EP coverage ratio for chromosomes 3, 7 and 13 of sample Linf_02A (top panel) and IGV snapshots of the respective chromosome extremities (bottom panel) is shown. The lower tracks (in order of appearance from the top) correspond to sequencing coverage in EP, sequencing coverage in EP+3, repeat elements or predicted low complexity regions predictions, and *L. infantum* gene annotations. The sequencing coverage tracks range from 0 to 500X. For chromosomes 7 and 13, the bottom panels highlight in orange the misassembled regions. **(C)** *SyntView* snapshot of chromosomes 7 and 13. From top to bottom the tracks show the orthologous genes in the *L. infantum* JPCM5, *L. donovani* BPK282A1, *L. donovani* PBQ71C8 and *L. major* Friedlin. Straight lines connect the orthologous genes in different genomes. The diagonal lines are indicative of misassembled genomic regions.

Supplementary Figures

Figure S1: Overview of experimental design. Clinical isolates were obtained from infected patients or dogs, placed in culture under standardized conditions and maintained for a defined number of passages *in vitro*. Promastigotes from logarithmic culture at passage 2 (early passage EP) or passage 5 (EP+3) were subjected to sequencing analysis to monitor the

dynamics of genomic adaptation to the culture environment. For certain strains, two independent cell cultures were derived for EP+3 to test for reproducibility of genome adaptation between biological replicates (EP+3.1 and EP+3.2).

Figure S2: Species validation. The genomic distance between the *Leishmania* isolates used in this study and the indicated *Leishmania* reference assemblies is shown by the PCA **(A)** and clustering analyses **(B)**. In the PCA plot the *L. donovani* and the *L. major* clusters are respectively highlighted in green and cyan.

Figure S3: Chromosome coverage analysis. **(A)** *Circos* plot representing the normalized sequencing coverage of the strains indicated. The bar height correlates with sequencing coverage. The coverage is shown on the vertical axis and ranges from 0 to 3. The ticks, scaled to represent 100Kb, show the genomic position. Green, early passage EP; orange, EP+3.1 replicate; purple, EP+3.2 replicate. **(B)** Zoom of Lmj_1948 chromosomes 10, 11, 14, 24, 26, 27 and 35.

Figure S4: Chromosome-specific gene coverage variation analysis. For each sample and for each chromosome the scatter plots show the normalized gene coverage for EP+3 (y-axis) versus EP (x-axis). The red diagonal lines indicate the bisectors. To show the extent of gene CNV with respect to the reference genomes, the axes limits are not fixed but dynamically assigned for each chromosome to include the maximum and the minimum measured values.

Figure S5: Chromosome-specific bin coverage variation analysis. Dots represent adjacent genomic intervals of 300 bases. For each sample, separate panels represent different

chromosomes. The x-axis in each panel represents the genomic coordinates while the y-axis indicates the normalized sequencing coverage. Intervals with coverage superior to two are highlighted in orange, and scores > 3 are assigned to 3. Intervals with coverage lower than 0.5 are highlighted in blue.

Table 1: Selection of gene CNVs in *L. infantum* field isolates (see full data in S7 Table)

L. infantum				
gene_id	**Linf_ZK27**	**Linf_LLM56**	**Linf_02A**	**annotation**
LinJ.08.0780	0.96	1.12	2.18	amastin-like protein
LinJ.09.0200	5.72	9.86	8.1	putative ATG8/AUT7/APG8/PAZ2
LinJ.10.0490*	18.1	20.55	32.92	GP63, leishmanolysin
LinJ.12.0661	11.63	13.46	6.1	conserved hypothetical protein
LinJ.15.1240	1.96	3.82	3.87	putative nucleoside transporter 1
LinJ.19.0820	9.58	14.39	9.09	putative ATG8/AUT7/APG8/PAZ2
LinJ.23.1330	2.45	3.44	1.46	hypothetical protein, unknown function
LinJ.26.snoRNA1	3.25	3.77	4.91	ncRNA
LinJ.26.snoRNA15	4.2	4.74	6.21	ncRNA
LinJ.26.snoRNA2	3.59	4.34	5.51	ncRNA
LinJ.26.snoRNA3	3.92	4.67	6.04	ncRNA
LinJ.26.snoRNA4	4.03	5	6.28	ncRNA
LinJ.26.snoRNA5	3.94	4.94	6.2	ncRNA
LinJ.26.snoRNA6	4.41	5.04	6.61	ncRNA
LinJ.26.snoRNA7	4.64	5.18	6.9	ncRNA
LinJ.29.0060*	2.04	1.08	0.96	putativetryptophanyl-tRNAsynthetase
LinJ.29.0070*	2.17	1.02	1.01	QA-SNARE protein putative
LinJ.29.0080*	2.07	1.08	0.99	conserved hypothetical protein
LinJ.29.0090*	2.09	1.03	1.05	putativeras-like small GTPases
LinJ.29.1610	1.89	4.45	1.81	conserved hypothetical protein
LinJ.29.2570	3.2	2.41	1.92	putative 60S ribosomal protein L13
LinJ.30.2990*	0.98	3.57	2.01	G3P dehydrogenase
LinJ.31.1470	1.98	1.96	1.17	hypothetical protein, unknown function
LinJ.31.1930	10.41	16.79	15.38	ubiquitin-fusion protein
LinJ.31.2390	1.04	1.04	0	helicase-like protein
LinJ.33.0360	20.87	13.19	12.22	heat shock protein 83-1
LinJ.34.1020	2.11	1.22	2.16	putative amastin-like surface protein
LinJ.34.1680	4.07	6.09	3.99	putative amastin-like surface protein
LinJ.36.0190	3.1	5.62	7.22	elongation factor 2

**, genes shown in Fig 2, right panel*

Table 2: Selection of gene CNVs in *L. donovani* field isolates (see full data in S7 Table)

L. donovani				
gene_id	**Ldo_CH33**	**Ldo_BPK26**	**Ldo_LTB**	**annotation**
LdBPK_040006600	6.17	0.94	4.8	hypothetical protein, conserved
LdBPK_050017700	14.07	12.32	9.35	snoRNA
LdBPK_080012500	10.68	9.38	7	amastin-like protein
LdBPK_080013600	7.46	4.69	4.1	amastin-like protein
LdBPK_080015900	7.21	10.48	6.93	cathepsin L-like protease
LdBPK_090006900	8.63	4.22	9.44	putative ATG8/AUT7/APG8/PAZ2
LdBPK_100009300	4.49	15.24	5.36	folate/biopterin transporter, putative
LdBPK_120013500	10.18	7.52	18.83	surface antigen protein 2, putative
LdBPK_120014600	18.73	8.8	15.23	hypothetical protein
LdBPK_190014300	11.45	7.24	13.77	putative ATG8/AUT7/APG8/PAZ2
LdBPK_270021500	2.11	4.16	3.06	amino acid transporter, putative
LdBPK_270026500	3.24	1.13	5.69	amino acid aminotransferase, putative
LdBPK_270030100	21.94	10.67	6.68	18S,ribosomal,SSU,RNA
LdBPK_270030130	20.81	10.7	6.4	rRNA
LdBPK_270030140	21.2	10.73	6.74	28S, ribosomal,RNA,LSU-alpha
LdBPK_270030150	19.96	9.97	6.18	28S, ribosomal,RNA,LSU-beta
LdBPK_270030160	17.77	9.65	5.93	28S, ribosomal,RNA,LSU-delta,M2
LdBPK_270030170	21.2	10.74	6.19	28S, ribosomal,RNA,LSU-zeta, M6
LdBPK_270030180	17.68	10.16	5.37	28S, ribosomal,RNA,LSU-epsilon,M4
LdBPK_280010700	3.08	1.01	2.48	major surface protease gp63, putative
LdBPK_280035000	8.59	14.66	8.04	heat-shock protein hsp70, putative
LdBPK_300020900	2.34	7.56	1.88	p1/s1 nuclease
LdBPK_310009700	7.22	10.63	6.01	amastin, putative
LdBPK_310016700	4.3	8.48	5.34	sodiumstibogluconate resistance protein
LdBPK_320043700	3.28	2.02	5.44	HIBCH-like protein
LdBPK_330008700	8.56	13.64	7.76	heat shock protein 83-17
LdBPK_340015500*	0.07	1.18	0.36	amastin-like surface protein, putative
LdBPK_340015600	3.19	5.12	3.15	amastin-like surface protein, putative
LdBPK_340015800	1.78	0.92	3.36	amastin-like surfaceprotein,putative
LdBPK_340017400	2.75	1.04	0.8	amastin-like surface protein, putative
LdBPK_340023500	3.03	1.87	9.92	amastin-like surface protein, putative
LdBPK_340024100*	1.47	26.05	5.71	Amastin surface glycoprotein, putative
LdBPK_350056400*	1	1	48.78	hypothetical protein
LdBPK_350056500*	1.02	1.07	47.88	hypothetical protein, conserved
LdBPK_350056600*	1.04	0.98	44.76	Protein-only RNaseP, putative
LdBPK_350056700*	1.22	1.1	36.57	Ribosomal protein L37e, putative
LdBPK_350056800*	1.03	1.03	43.11	RNA pseudouridylate synthase, putative
LdBPK_350056900*	1.01	0.91	45.34	hypothetical protein
LdBPK_350057000*	0.92	0.96	41.41	hypothetical protein
LdBPK_350057100*	1.05	0.87	42.65	hypothetical protein, unknown function
LdBPK_350057200*	0.97	0.96	43.22	biopterin transporter, putative
LdBPK_350057300*	1.06	0.89	44	hypothetical protein

**, genes shown in Fig 2, right panel*

Table 3: Gene CNVs in the Spanish *L. infantum* isolates Linf_LLM45 and Linf_LLM56

gene	45*	56*	Ratio	delta	annotation
LinJ.02.0690	1.6	2.1	0.7	0.5	hypothetical protein, unknown function
LinJ.03.0420	1.4	1.9	0.7	0.6	putative 60S acidic ribosomal protein P2
LinJ.04.0160	1.4	2.0	0.7	0.6	hypothetical protein
LinJ.04.0180	2.2	1.1	2.0	1.1	surface antigen-like protein
LinJ.05.snoRNA3	7.9	8.4	0.9	0.6	ncRNA
LinJ.05.snoRNA5	7.7	8.8	0.9	1.1	ncRNA
LinJ.09.0200	8.8	7.8	1.1	1.0	atg8 aut7 apg8 paz2. Cytoskeleton
LinJ.10.0490	15.4	16.7	0.9	1.3	GP63, leishmanolysin
LinJ.11.1110	3.3	1.9	1.7	1.4	putative 60S ribosomal protein L28
LinJ.11.1120	2.1	1.0	2.1	1.1	conserved hypothetical protein
LinJ.13.0330	11.3	10.0	1.1	1.3	alpha tubulin
LinJ.14.0400	1.8	3.8	0.5	2.0	conserved hypothetical protein
LinJ.15.snoRNA4	15.3	13.8	1.1	1.5	ncRNA
LinJ.17.0090	21.1	21.8	1.0	0.8	elongation factor 1-alpha
LinJ.18.1500	4.0	3.1	1.3	0.9	putative P-type H+-ATPase
LinJ.19.0820	9.9	11.3	0.9	1.4	putative ATG8/AUT7/APG8/PAZ2
LinJ.19.1350	2.7	3.8	0.7	1.0	putative glycerol uptake protein
LinJ.22.snoRNA1	5.7	4.7	1.2	1.0	ncRNA
LinJ.26.snoRNA10	5.4	4.9	1.1	0.5	ncRNA
LinJ.26.snoRNA15	5.4	4.7	1.1	0.6	ncRNA
LinJ.26.snoRNA7	5.8	5.2	1.1	0.7	ncRNA
LinJ.29.1570	1.0	1.6	0.7	0.5	conserved hypothetical protein
LinJ.29.1580	1.0	1.5	0.7	0.5	conserved hypothetical protein
LinJ.29.1610	2.8	3.7	0.8	0.9	conserved hypothetical protein
LinJ.29.2240	1.2	1.8	0.6	0.6	conserved hypothetical protein
LinJ.30.0690	3.6	3.0	1.2	0.6	putative 40S ribosomal protein S30
LinJ.30.1660	2.0	1.4	1.4	0.6	conserved hypothetical protein
LinJ.30.3550	1.0	2.0	0.5	1.0	conserved hypothetical protein
LinJ.30.3560	1.0	2.0	0.5	1.0	S-adenosylmethioninesynthetase
LinJ.31.0460	3.0	1.0	2.9	2.0	putative amastin
LinJ.31.1660	2.9	2.1	1.4	0.8	3-ketoacyl-CoA thiolase-like protein
LinJ.31.1930	16.1	13.4	1.2	2.7	ubiquitin-fusion protein
LinJ.32.1910	2.8	1.8	1.6	1.0	putative iron superoxide dismutase
LinJ.33.0360	5.8	11.3	0.5	5.6	heat shock protein 83-1
LinJ.34.1010	5.4	3.8	1.4	1.6	putative amastin-like surface protein
LinJ.34.1020	3.1	1.2	2.6	1.9	putative amastin-like surface protein
LinJ.34.1680	4.1	6.1	0.7	2.0	putative amastin-like surface protein
LinJ.34.1730	10.9	14.4	0.8	3.5	putative amastin-like surface protein
LinJ.36.0190	6.0	5.0	1.2	1.0	elongation factor 2
LinJ.36.1680	1.8	2.5	0.7	0.6	universalminicirclesequence bd. protein
LinJ.36.3010	1.5	2.3	0.7	0.8	40S ribosomal protein S24e

** normalized mean read depth of Linf_LLM45 and Linf_LLM56*

Bussotti et al_Fig1

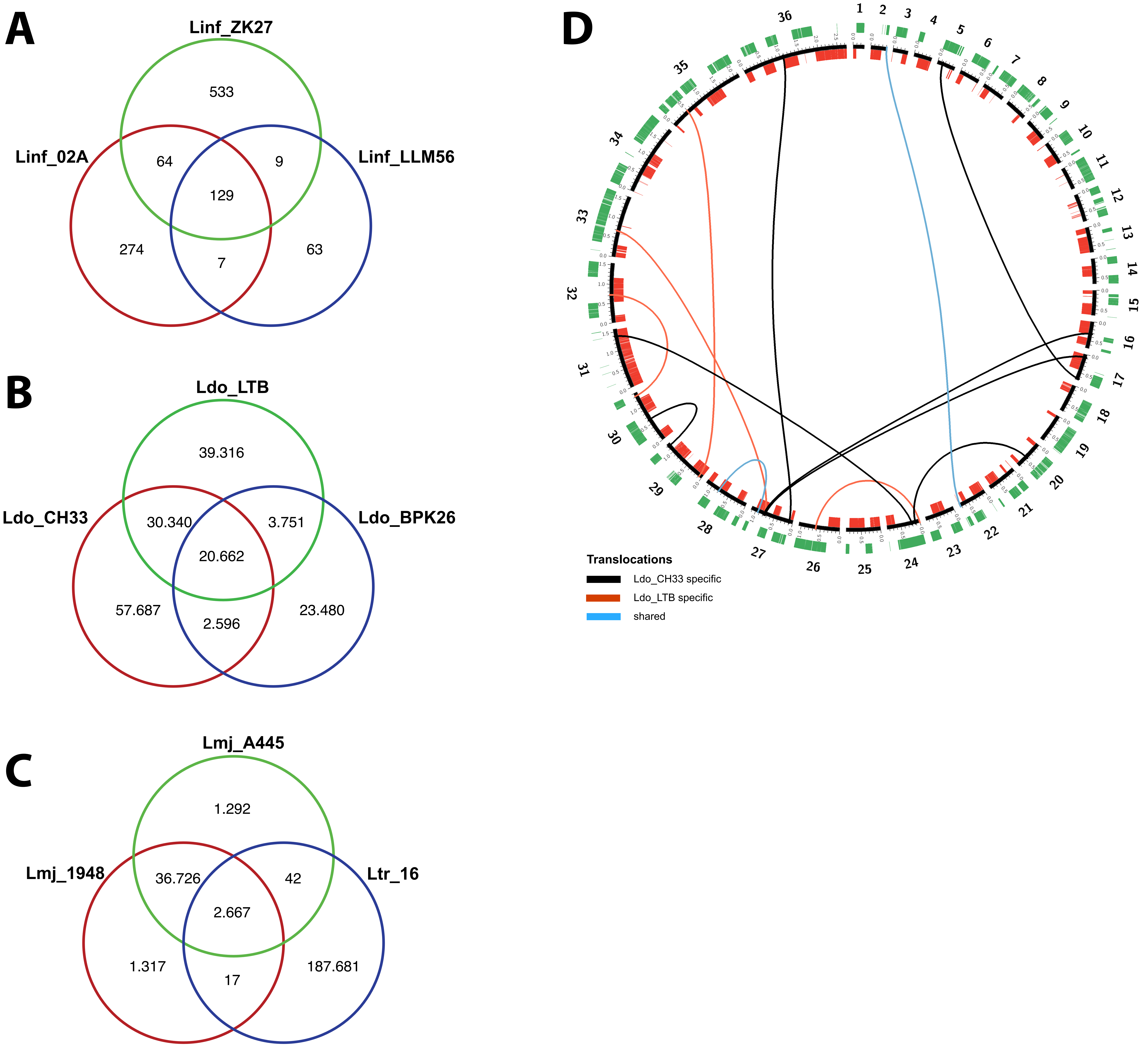

Bussotti et al_Fig2

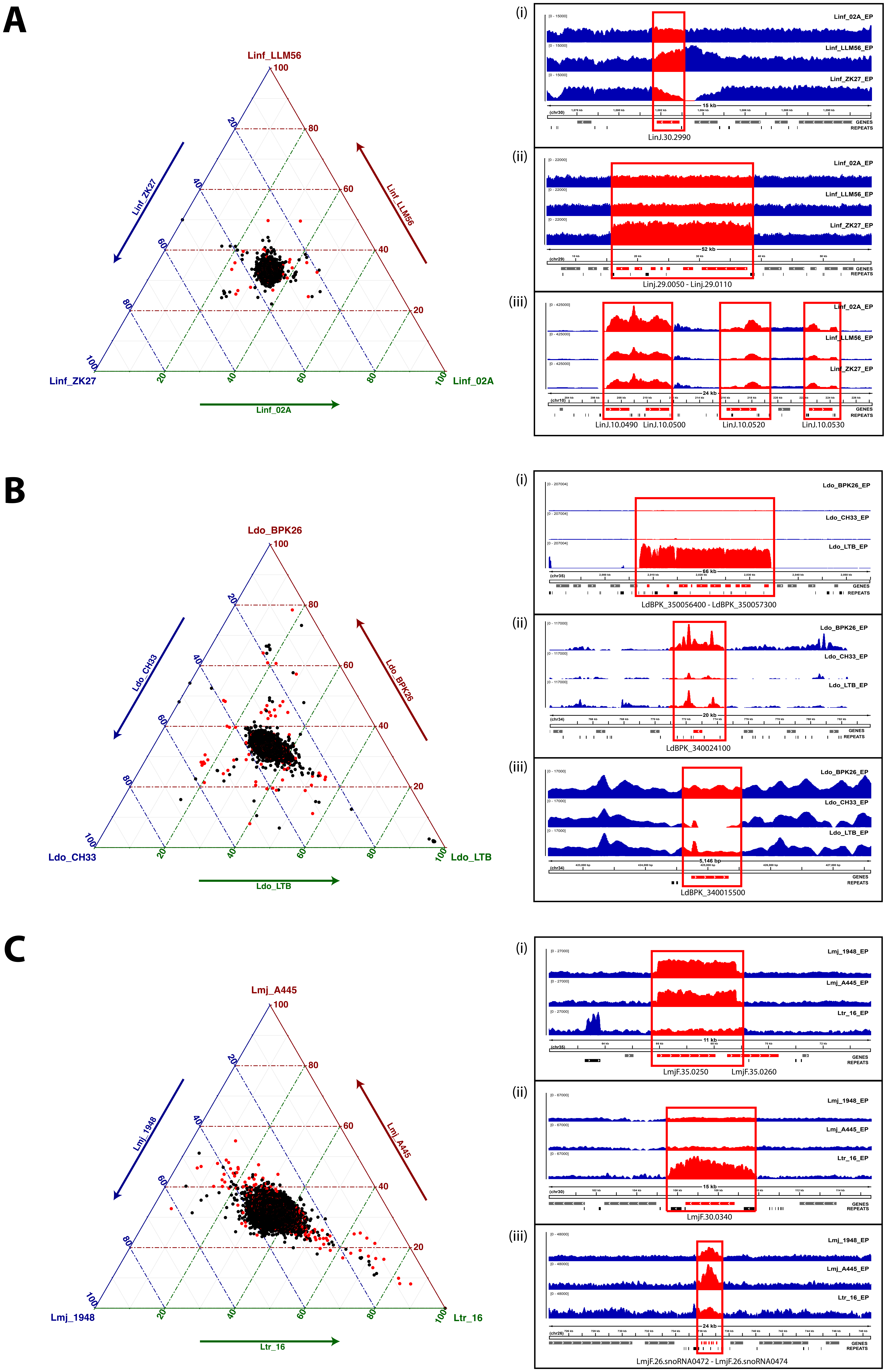

Bussotti et al_Fig3

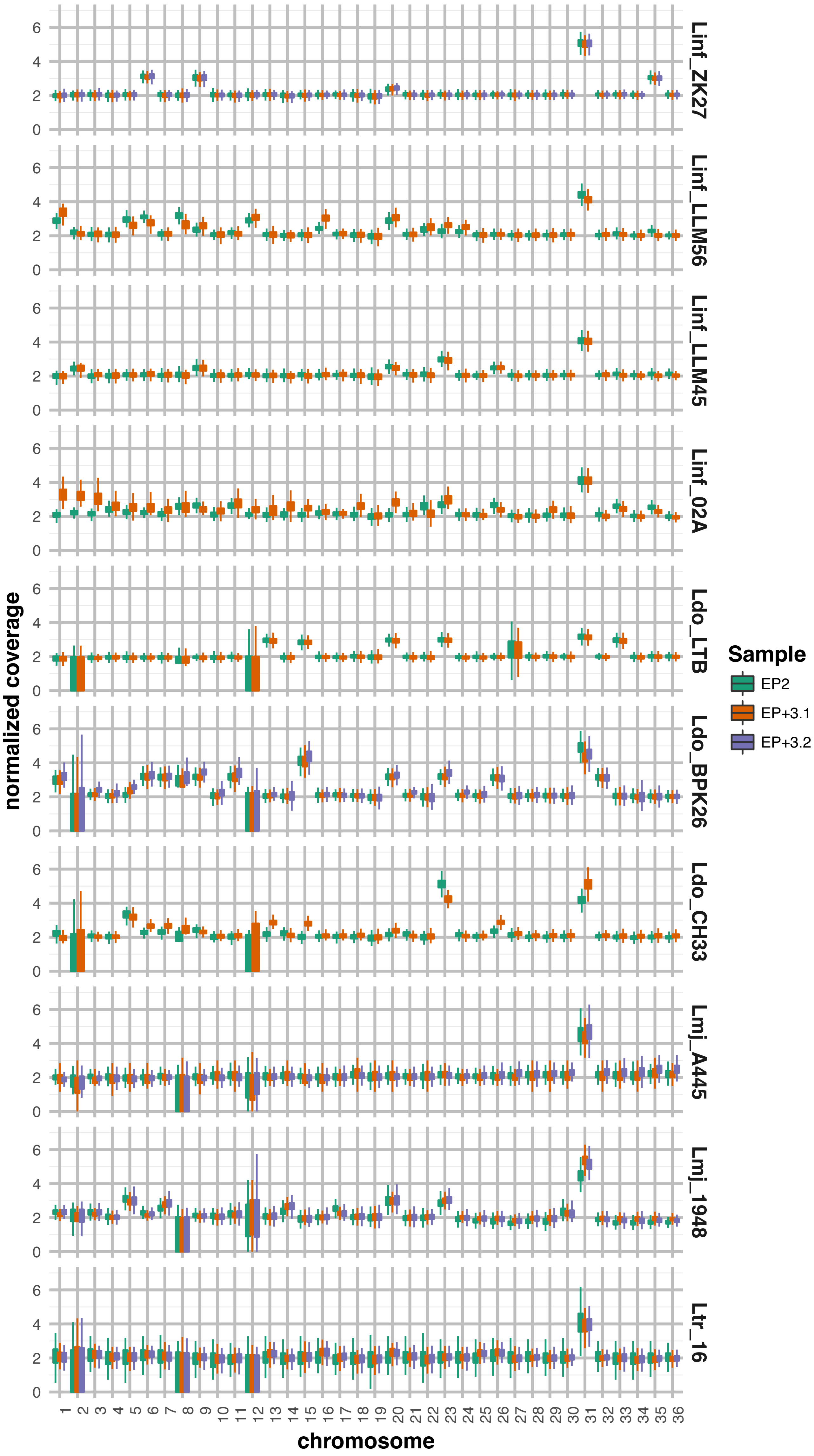

Bussotti et al_Fig4

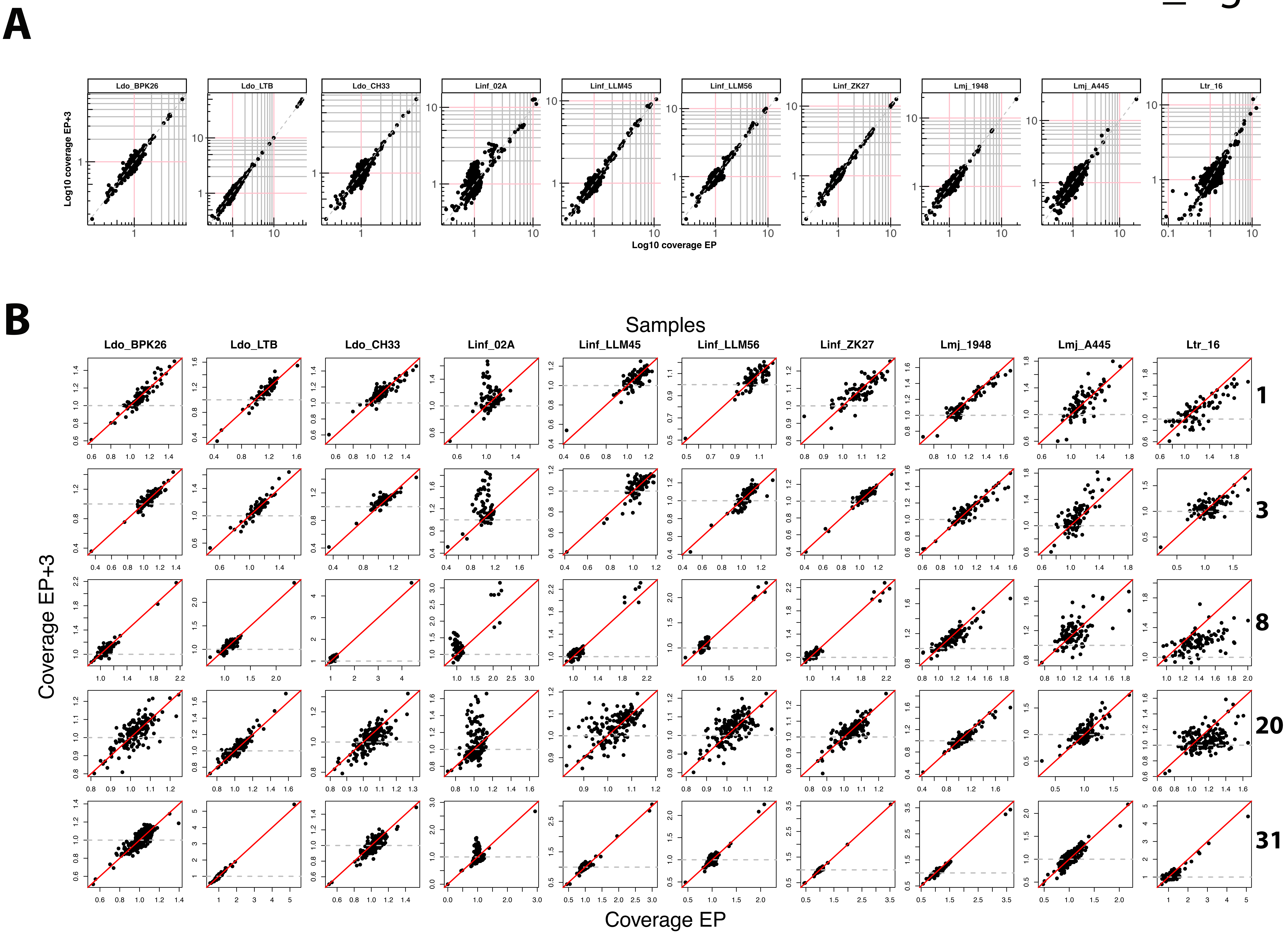

Bussotti et al_Fig5

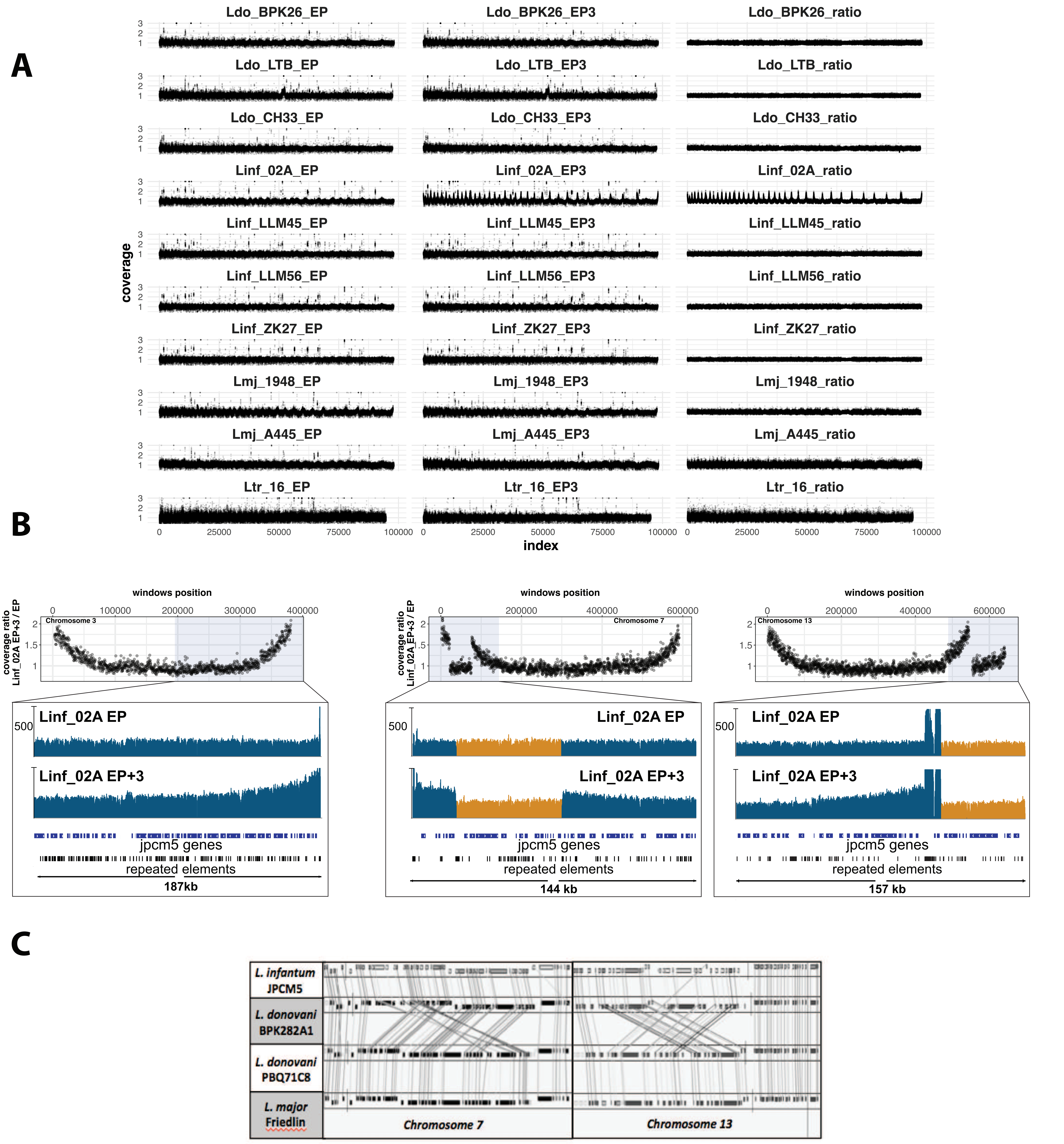
A
Ldo_BPK26_EP
Ldo_BPK26_EP3
Ldo_BPK26_ratio
Ldo_LTB_EP
Ldo_LTB_EP3
Ldo_LTB_ratio
Ldo_CH33_EP
Ldo_CH33_EP3
Ldo_CH33_ratio
Linf_02A_EP
Linf_02A_EP3
Linf_02A_ratio
Linf_LLM45_EP
Linf_LLM45_EP3
Linf_LLM45_ratio
Linf_LLM56_EP
Linf_LLM56_EP3
Linf_LLM56_ratio
Linf_ZK27_EP
Linf_ZK27_EP3
Linf_ZK27_ratio
Lmj_1948_EP
Lmj_1948_EP3
Lmj_1948_ratio
Lmj_A445_EP
Lmj_A445_EP3
Lmj_A445_ratio
Ltr_16_EP
Ltr_16_EP3
Ltr_16_ratio
coverage
index
B
windows position
coverage ratio
Linf_02A EP+3 / EP
Chromosome 3
Linf_02A EP
Linf_02A EP+3
jpcm5 genes
repeated elements
187kb
windows position
Chromosome 7
Linf_02A EP
Linf_02A EP+3
jpcm5 genes
repeated elements
144 kb
windows position
Chromosome 13
Linf_02A EP
Linf_02A EP+3
jpcm5 genes
repeated elements
157 kb
C
L. infantum
JPCM5
L. donovani
BPK282A1
L. donovani
PBQ71C8
L. major
Friedlin
Chromosome 7
Chromosome 13